Journal of Mathematical Biology (2020) 81:875–904
https://doi.org/10.1007/s00285-020-01530-w

Mathematical Biology

An integrodifference model for vegetation patterns in semi-arid environments with seasonality

Lukas Eigentler[1,2,3] · Jonathan A. Sherratt[1]

Received: 9 May 2019 / Revised: 4 March 2020 / Published online: 4 September 2020

Abstract
Vegetation patterns are a characteristic feature of semi-deserts occurring on all continents except Antarctica. In some semi-arid regions, the climate is characterised by seasonality, which yields a synchronisation of seed dispersal with the dry season or the beginning of the wet season. We reformulate the Klausmeier model, a reaction–advection–diffusion system that describes the plant–water dynamics in semi-arid environments, as an integrodifference model to account for the temporal separation of plant growth processes during the wet season and seed dispersal processes during the dry season. The model further accounts for nonlocal processes involved in the dispersal of seeds. Our analysis focusses on the onset of spatial patterns. The Klausmeier partial differential equations (PDE) model is linked to the integrodifference model in an appropriate limit, which yields a control parameter for the temporal separation of seed dispersal events. We find that the conditions for pattern onset in the integrodifference model are equivalent to those for the continuous PDE model and hence independent of the time between seed dispersal events. We thus conclude that in the context of seed dispersal, a PDE model provides a sufficiently accurate description, even if the environment is seasonal. This emphasises the validity of results that have previously been obtained for the PDE model. Further, we numerically investigate the effects of changes to seed dispersal behaviour on the onset of patterns. We find that long-range seed dispersal inhibits the formation of spatial patterns and that the seed dispersal kernel's decay at infinity is a significant regulator of patterning.

Keywords Pattern formation · Integrodifference model · Nonlocal dispersal · Seasonal environments · Semi-arid landscapes

Mathematics Subject Classification 39A23 · 39A30 · 37N25 · 92D40

Lukas Eigentler was supported by The Maxwell Institute Graduate School in Analysis and its Applications, a Centre for Doctoral Training funded by the UK Engineering and Physical Sciences Research Council (Grant EP/L016508/01), the Scottish Funding Council, Heriot-Watt University and the University of Edinburgh.

Extended author information available on the last page of the article

1 Introduction

Vegetation patterns are a ubiquitous feature of ecosystems in semi-arid climate zones. Occurrences of such mosaics of plants and bare soil have been reported from all continents except Antarctica, including the African Sahel (Deblauwe et al. 2012) and the Horn of Africa (Gowda et al. 2018), Western Australia (Gandhi et al. 2018), northern Chile (Fernandez-Oto et al. 2019), Israel (Sheffer et al. 2013), the Chihuahuan Desert in North America (Deblauwe et al. 2012) and Southeastern Spain (Lesschen et al. 2008). A detailed understanding of the evolution of vegetation patterns is of considerable importance as they hold valuable information on the health of ecosystems. For example, changes to a pattern's properties such as its wavelength, its recovery time from perturbations, or the area fraction covered by biomass can act as early warning signals of desertification (Corrado et al. 2014; Dakos et al. 2011; Gowda et al. 2016; Kéfi et al. 2007; Rietkerk et al. 2004; Saco et al. 2018; Zelnik et al. 2018). Desertification processes are a major threat to economies in semi-deserts as agriculture provides a significant contribution to GDP (United Nations Convention to Combat Desertification 2017). For example, the livestock sector, which depends in part on animals grazing on spatially patterned vegetation, accounts for 20% of GDP in Chad and involves 40% of its population (Dickovick 2014; United Nations Food and Agriculture Organization 2005).

A number of feedback mechanisms may be involved in the pattern formation process (see Meron 2018 for a review), but it is widely agreed that a central mechanism is the vegetation-infiltration feedback loop, which results in a redistribution of water towards areas of high biomass. On bare soil, the formation of physical and biological soil crusts inhibits water infiltration into the soil (Eldridge et al. 2000). Thus, water run-off towards existing vegetation patches occurs. The enhancement of environmental conditions in these sinks for the limiting resource drives further plant growth and thus closes the feedback loop (Thompson et al. 2010).

Dryland plants have developed a range of seed production and dispersal strategies to cope with the environmental stress in their habitats (Ellner and Shmida 1981; van Rheede van Oudtshoorn and van Rooyen 2013). One such mechanism, commonly observed in water-controlled ecosystems, is ombrohydrochory, the dispersal of seeds caused by an opening of the seed container due to contact with water (Parolin 2006; Navarro et al. 2009; van Rheede van Oudtshoorn and van Rooyen 2013). One particular form, exhibited by members of the Aizoaceae family in semi-arid regions of the Sahel, Australia and South America, is ballistic dispersal, which uses the kinetic energy of raindrops to expulse the plants' seeds (Parolin 2006; Friedman et al. 1978). Some semi-arid environments such as those in the Mediterranean are characterised by seasonal fluctuations in their environmental conditions and in particular in their precipitation patterns (Noy-Meir 1973). In combination with processes that allow plants to store diaspores during periods of drought, ombrohydrochory yields a synchronisation of seed dispersal with the beginning of the wet season in such seasonal environments. This synchronisation has, for example, been reported in *Mesembryanthemum crystallinum* and *Mesembryanthemum nodiflorum* in Southeastern Spain (Navarro et al. 2009). If seed dispersal strategies different from ombrohydrochory are dominant, most species disperse their seeds during the dry season (Navarro et al. 2009; Shabana et al. 2018).

The seasonal synchronisation of seed dispersal splits the annual life-cycle of a plant population into two distinct stages. During the wet season, seeds germinate, new seedlings emerge and adult plants increase their biomass, but no spatial movement takes place. Seed dispersal only occurs during, or at the end of the dry season, while growth processes are dormant (Baudena and Provenzale 2008). By contrast, most mathematical models for dryland vegetation patterns consist of partial differential equations and thus assume that seed dispersal occurs continuously in time. A widely used approach to account for the temporal structure of the annual life cycle is the use of integrodifference equations. This splits the system into 2 distinct, non-overlapping phases, which are both described as discrete, instantaneous processes: a growth phase during which dispersal processes are either not present or negligible and a dispersal phase during which no growth occurs. The application of integrodifference equations to biological and ecological systems in which spatial dispersal plays a significant role was in part pioneered by Kot and Schaffer (1986), and has become a well-established tool in the description of biological and ecological systems since then [e.g. by Musgrave and Lutscher (2014a), Musgrave and Lutscher (2014b), Powell and Zimmermann (2004), Clark et al. (2003), Neubert et al. (1995)].

The spatial and temporal scales associated with the evolution of vegetation patterns do not allow their recreation in laboratory settings. Instead, a range of mathematical models have been proposed to address different aspects of the pattern dynamics (Borgogno et al. 2009; Zelnik et al. 2013). A significant amount of modelling work is based on systems of partial differential equations, most notably by Gilad et al. (2004), HilleRisLambers et al. (2001); Rietkerk et al. (2002) and Klausmeier (1999). The reaction-advection-diffusion Klausmeier model (Klausmeier 1999) is a deliberately basic description of dryland ecosystems based on the vegetation-infiltration feedback loop. Its relative simplicity provides a rich framework for model analyses and extensions [e.g. the work by Bennett and Sherratt (2018), Consolo et al. (2019), Eigentler and Sherratt (2018), Eigentler and Sherratt (2019), Siteur et al. (2014a), Ursino and Contarini (2006), Sherratt (2010), Sherratt (2011), Sherratt (2013a), Sherratt (2013b), Sherratt (2013c)]. The recent development of new remote sensing technology, using temporal sequences of satellite images, allows for comparisons between model predictions and field data (Bastiaansen et al. 2018; Gandhi et al. 2018).

In the Klausmeier model, seed dispersal is modelled by a diffusion term. In reality, the dispersal of seeds is affected by nonlocal processes, such as ballistic dispersal or long range dispersal (e.g. via mammals or wind) (Pueyo et al. 2008; Bullock et al. 2017). The Klausmeier model has been extended to account for such nonlocal processes (Eigentler and Sherratt 2018; Bennett and Sherratt 2018) and a similar approach has been applied to other models for dryland vegetation (Baudena and Rietkerk 2013; Pueyo et al. 2008, 2010). Integrodifference systems also provide a description of nonlocal dispersal effects through a convolution of the plant density with a kernel function. The kernel function is a probability density function describing the average distribution of seeds dispersed from a single plant. The dispersal kernel's properties (in particular its shape and standard deviation) depend on both plant species and environmental conditions (Bullock et al. 2017).

In this paper we address the significance of seed dispersal synchronisation and its temporal separation from growth processes in seasonal dryland environments. To do

so, we introduce an integrodifference model describing the plant–water dynamics in semi-arid ecosystems in Sect. 2. We base our model on the Klausmeier model, to compare our results to previous model analyses of models with no temporal structure. To aid comparisons to the PDE model, we review the most relevant results for the Klausmeier model in Sect. 2. Even though an integrodifference model cannot explicitly take into account the length of the plant growth stage, a consistency result (Proposition 1) yields a control parameter for the temporal separation of seed dispersal events through an appropriate parameter setting. In Sect. 3 we focus on this special case and perform a linear stability analysis to determine a condition for pattern onset in the model and investigate this condition under variations in the growth season length. The analytical derivation of this condition relies on a specific (but nevertheless biologically relevant) choice of the dispersal kernels. To relax this assumption we perform numerical simulations in Sect. 4 to determine the parameter region in which pattern onset occurs for other biologically relevant dispersal kernels. Finally, we discuss our results in Sect. 5.

2 The models

In this section we introduce the integrodifference model which we use to investigate the effects of seasonal synchronisation of seed dispersal on the onset of vegetation patterns in semi-arid environments. The model is based on the reaction-advection-diffusion model by Klausmeier (1999) and to facilitate the comparison of our results on the discrete model to that of the time-continuous model, we start by reviewing relevant results for the Klausmeier model. We relate the models through a convergence result that shows that the Klausmeier PDE model can be obtained from the integrodifference model in an appropriate limit.

2.1 Klausmeier model

One of the well-established models describing vegetation patterns in semi-arid environments is the Klausmeier model (Klausmeier 1999). It reduces the plant–water dynamics to a small set of basic processes (rainfall, plant mortality, evaporation/drainage, vegetation-infiltration feedback and spatial dispersal). The relative simplicity of this modelling approach provides a framework for a rich mathematical analysis [e.g. by Sherratt (2005), Sherratt and Lord (2007), Sherratt (2010), Sherratt (2011), Sherratt (2013a), Sherratt (2013b), Sherratt (2013c), Siteur et al. (2014a), Ursino and Contarini (2006)]. Suitably nondimensionalised (Klausmeier 1999; Sher-

ratt 2005), the model is

$$\frac{\partial u}{\partial t} = \overbrace{u^2 w}^{\text{plant growth}} - \overbrace{Bu}^{\text{plant mortality}} + \overbrace{\frac{\partial^2 u}{\partial x^2}}^{\text{plant dispersal}}, \tag{1a}$$

$$\frac{\partial w}{\partial t} = \underbrace{A}_{\text{rainfall}} - \underbrace{w}_{\substack{\text{evaporation}\\ \text{and drainage}}} - \underbrace{u^2 w}_{\substack{\text{water consumption}\\ \text{by plants}}} + \underbrace{\nu \frac{\partial w}{\partial x}}_{\substack{\text{water flow}\\ \text{downhill}}} + \underbrace{d \frac{\partial^2 w}{\partial x^2}}_{\text{water diffusion}}. \tag{1b}$$

Here $u(x,t)$ denotes the plant density, $w(x,t)$ the water density, $x \in \mathbb{R}$ the space domain where x is increasing in the uphill direction and $t > 0$ the time. Originally, the model only focussed on a sloped spatial domain, but the addition of a water diffusion term to account for the possibility of a description on flat terrain is a well established addition (Kealy and Wollkind 2012; Siteur et al. 2014a; van der Stelt et al. 2013; Zelnik et al. 2013). To emphasise on the description of seed dispersal as a local process, we refer to this model as the "local Klausmeier model" throughout the paper. Water input to the system is assumed to occur at a constant rate, evaporation and drainage effects are proportional to the water density (Rodriguez-Iturbe et al. 1999; Salvucci 2001) and the plant mortality rate is density-independent. The nonlinearity in the description of water uptake and plant growth processes arises due to a soil modification by plants. The term is the product of the density of the consumer u and of the available resource uw, the amount of water that is able to infiltrate into soil layers where plant roots consume water. The dependence on the plant density u in the latter term occurs due to a positive correlation between the plant density and the soil surface's permeability (Rietkerk et al. 2000; Valentin et al. 1999; Cornet et al. 1988). Finally, plant growth is assumed to be proportional to the amount of consumed water (Rodriguez-Iturbe et al. 1999; Salvucci 2001). The parameters A, B, ν and d are combinations of different dimensional parameters but can be interpreted as rainfall, plant loss, the slope and water diffusion, respectively.

In a previous paper (Eigentler and Sherratt 2018) we have introduced nonlocal seed dispersal effects to the model by replacing the plant diffusion term by a convolution of a dispersal kernel (a probability density function) ϕ and the plant density u. The resulting model is referred to as the "nonlocal Klausmeier model" and is

$$\frac{\partial u}{\partial t} = u^2 w - Bu + C\left(\phi(\cdot) * u(\cdot,t) - u(x,t)\right), \tag{2a}$$

$$\frac{\partial w}{\partial t} = A - w - u^2 w + \nu \frac{\partial w}{\partial x} + d \frac{\partial^2 w}{\partial x^2}. \tag{2b}$$

The additional parameters C and a represent the rate of plant dispersal and reciprocal width of the dispersal kernel, respectively. Note that the convolution $(\phi * u)(x,t)$ accounts for all plant biomass dispersed to the space point x, including the fraction of biomass that is not dispersed. The final term in (2a) ensures that the total biomass over the whole domain remains unchanged by the seed dispersal term. The nonlocal model (2) and the local model (1) are related through a convergence result. If the

dispersal kernel ϕ is decaying exponentially as $|x| \to \infty$, then the local model (1) can be obtained from the nonlocal model (2) in the limit $C \to \infty$ and $\sigma \to 0$ with $C = 2/\sigma^2$, where σ denotes the standard deviation of ϕ (Eigentler and Sherratt 2018).

Linear stability analysis of both the local and the nonlocal Klausmeier model with the Laplace kernel

$$\phi(x) = \frac{a}{2} e^{-a|x|}, \quad a > 0, x \in \mathbb{R}. \tag{3}$$

provides analytically derived conditions for pattern onset to occur in the system. On flat ground, i.e. $\nu = 0$, Turing-type patterns form due to a diffusion-driven instability, i.e. there exists a threshold $d_c > 0$ on the diffusion coefficient such that an instability occurs for all $d > d_c$. In the local model (1), the threshold is

$$d_c(A, B) = \frac{8B\sqrt{-A^2 + A\sqrt{A^2 - 4B^2} + 4B^2} - 2A^2 + 2A\sqrt{A^2 - 4B^2} + 16B^2}{B\left(A - \sqrt{A^2 - 4B^2}\right)^2}. \tag{4}$$

A corresponding threshold $\widetilde{d_c}(A, B, C, a)$ for the nonlocal model (2) with the Laplace kernel (3) can be derived explicitly, but it omitted due to its algebraic complexity.

On sloped ground ($\nu \neq 0$) pattern onset has been studied close to a Turing-Hopf bifurcation, which is characterised by an upper bound on the rainfall parameter A that has been derived analytically valid to leading order in ν as $\nu \to \infty$ for both models (Eigentler and Sherratt 2018; Sherratt 2013b). The calculation of this upper bound on the precipitation parameter for the nonlocal model with the Laplace kernel shows that long range dispersal of seeds inhibits the formation of patterns by decreasing the size of the parameter region that supports the onset of patterns. On flat ground an increase of the dispersal kernel's standard deviation causes an increase in the threshold on the diffusion coefficient, while on sloped ground an increase in the dispersal kernel's width inhibits the formation of patterns by decreasing the upper bound on the rainfall parameter.

The analytical derivation of pattern onset conditions in the nonlocal model is facilitated by the simple algebraic form of the Laplace kernel's Fourier transform and the associated polynomial structure of the dispersion relation in the linear stability analysis. For other biologically relevant seed dispersal kernels, conditions for pattern onset are not analytically tractable. Numerical simulations, however, confirm the qualitative trends obtained for the model with the Laplace kernel. Simulations further suggest that the dispersal kernel's decay at infinity has an influence on the rainfall threshold. For narrow dispersal kernels, those that account for more rare long-range dispersal events (algebraic decay rather than exponential) have an inhibitory effect on the formation of patterns, while for sufficiently wide kernels those that decay algebraically at infinity promote pattern formation compared to exponentially decaying kernels.

2.2 Integrodifference model

Integrodifference models are a common type of model widely used in the description of systems in which dispersal processes are temporally separated from other dynamics such as growth/birth and decay/death. To account for the separation of plant growth and seed dispersal stages in dryland ecosystems, we propose the integrodifference model

$$u_{n+1}(x) = C\phi * f(u_n, w_n), \tag{5a}$$
$$w_{n+1}(x) = D\phi_1 * g(u_n, w_n), \tag{5b}$$

where

$$f(u, w) = u^2 w - Bu + \frac{1}{C}u,$$
$$g(u, w) = A - u^2 w - w + \frac{1}{D}w.$$

Here $u_n(x)$ denotes the plant density, $w_n(x)$ the water density after $2n$, $n \in \mathbb{N}$ seasons and location $x \in \mathbb{R}$, where x increases in the uphill direction. The formulation of the model splits the processes involved into two phases: a growth and evolution phase described by the functions $f(u, w)$ and $g(u, w)$ during which no dispersal occurs, and a dispersal phase modelled as a convolution of the evolved densities with dispersal kernels. As in the nonlocal Klausmeier model (2), the plant dispersal kernel ϕ is symmetric and represents isotropic dispersal of plants. To model the flow of water downhill, the water dispersal kernel ϕ_1 is in general asymmetric with mean $\mu_{\phi_1} \leq 0$. The special case of a symmetric kernel ϕ_1 corresponds to the model on flat ground, which is the main aspect of the study in this paper. The model is based on the Klausmeier models (2) and (1) and thus the functions $f(u, w)$ and $g(u, w)$ consist of the terms describing the rate of change in the original model, appropriately scaled by the coefficients C and D to reflect the time between steps in the discrete model, added to the existing densities.

As the integrodifference model (5) arises directly from the local Klausmeier model (1), the two models can be linked through a consistency result in an appropriate limit which shows that *the integrodifference model* (5) *tends to the local Klausmeier model* (1) as $T \to 0$. To show this, we consider the parameter setting

$$C = T, \quad \sigma_\phi^2 = 2T, \quad D = T, \quad \mu_{\phi_1} = -\nu T, \quad \widetilde{\sigma}_{\phi_1}^2 = 2dT, \tag{6}$$

where μ and σ denote the mean and standard deviation of the respective kernels and $\widetilde{\sigma}_{\phi_1}^2 = \int_{-\infty}^{\infty} \phi_1(x)x^2 \mathrm{d}x$, the second raw moment of the kernel function ϕ_1. Further, we define operators P, $P_T : C^\infty(\mathbb{R} \times [0, \infty), [0, \infty)^2) \to C^\infty(\mathbb{R} \times [0, \infty), [0, \infty)^2)$ by

$$P\boldsymbol{v}(x, t) = \frac{\partial \boldsymbol{v}}{\partial t}(x, t) - \Gamma \boldsymbol{v}(x, t) - h_1(\boldsymbol{v}(x, t)), \tag{7}$$

for any function $\boldsymbol{v}(x,t) = (u(x,t), w(x,t)) \in C^\infty(\mathbb{R} \times [0,\infty), [0,\infty)^2)$, where

$$\Gamma = \operatorname{diag}\left(\frac{\partial^2}{\partial x^2}, \nu\frac{\partial}{\partial x} + d\frac{\partial^2}{\partial x^2}\right), \quad h_1(\boldsymbol{v}) = \begin{pmatrix} u^2 w - Bu \\ A - u^2 w - w \end{pmatrix},$$

and

$$P_T \boldsymbol{v}(x,t) = \frac{1}{T}\left(\boldsymbol{v}(x,t+T) - h_2(\boldsymbol{v}(x,t))\right), \tag{8}$$

where

$$h_2(\boldsymbol{v}(x,t)) = \begin{pmatrix} -C\phi(\cdot) * f(u(\cdot,t), w(\cdot,t)) \\ -D\phi_1(\cdot) * g(u(\cdot,t), w(\cdot,t)) \end{pmatrix}.$$

Note that the operator P arises from the local Klausmeier model (1), because $P\boldsymbol{v} = 0$ for any $\boldsymbol{v}$ that satisfies (1). Similarly, P_T represents the integrodifference model (5), because a sequence $\boldsymbol{v}_n(x) = \boldsymbol{v}(x, nT)$ satisfies (5) if $P_T \boldsymbol{v}_n = 0$ for all $n \in \mathbb{N}$. Utilising this reformulation of both models, it is possible to show the following result.

Proposition 1 *Consider the parameter setting (6) and let the kernel functions ϕ and ϕ_1 have finite moments of all orders and decay exponentially as $|x| \to \infty$. Then the integrodifference model (5) is consistent with the local Klausmeier model (1), i.e.*

$$P\boldsymbol{v} - P_T \boldsymbol{v} \to 0 \quad \text{as} \quad T \to 0^+,$$

for any $\boldsymbol{v} \in C^\infty(\mathbb{R} \times [0,\infty), [0,\infty)^2)$.

In other words, the model equations (5) converge to the model equations (1) as $T \to 0^+$. The notion of *consistency* is widely used in the field of numerical analysis, and crucially it does not imply convergence of model solutions. While we are unable to construct an argument to prove convergence, numerical simulations suggest that solutions of the integrodifference model (5) converge to solutions of the local Klausmeier model (1) in the parameter setting (6) as $T \to 0^+$ (Fig. 2).

On sloped ground Proposition 1 requires that $\nu = o(T^{-1})$, so that $T\nu \to 0$ as $T \to 0^+$ and $\nu \to \infty$, to facilitate any asymptotic analysis in ν similar to that of the local Klausmeier model (Sherratt 2005, 2010, 2011, 2013a, b, c). On flat ground, ϕ_1 is symmetric and thus $\mu_{\phi_1} = 0$ and $\widetilde{\sigma}_{\phi_1}$ coincides with the kernel's standard deviation σ_{ϕ_1}.

The parameter T can be interpreted as the time between separate dispersal events and the scalings (6) are thus the main focus of the model's analysis in Sect. 3. While the time between two seed dispersal events in a seasonal environment is usually fixed, we are interested in variations of T as this parameter establishes a connection between the local Klausmeier model (1) and the integrodifference model (5). In particular, as $T \to 0^+$ in the model, the length of each season tends to zero. As a consequence, this limit corresponds to the disappearance of any seasonality in the model and all processes

are assumed to occur continuously in time, as, for example, in the Klausmeier model (1).

One kernel function satisfying the conditions in Proposition 1 is the Laplacian kernel (3). We define the corresponding asymmetric Laplace kernel by $\phi_1(x) = Ne^{-a_2 x}$ for $x \geq 0$ and $\phi_1(x) = Ne^{(a_2-a_1)x}$ for $x < 0$, where $N = (a_2-a_1)a_2/(2a_2-a_1)$ and $a_2 > a_1 > 0$. The parameter a_1 controls the extent of the asymmetry of the kernel function and $a_1 = 0$ yields the symmetric Laplace kernel (3). The model with this particular kernel function is studied in some detail in this paper as the Fourier transform of the symmetric Laplacian kernel $\widehat{\phi}(k) = a^2/(a^2+k^2)$ provides a significant simplification in the analysis of pattern onset.

Proof of Proposition 1 Firstly, we show that

$$P_T \boldsymbol{v}(x,t) = \frac{\boldsymbol{v}(x,t+T) - \boldsymbol{v}(x,t)}{T} - \Gamma \boldsymbol{v}(x,t) - h_1(\boldsymbol{v}(x,t)) + O\left(T^2\right). \tag{9}$$

To this end, we define $\phi(x) = \sigma_\phi^{-1}\varphi(\sigma_\phi^{-1}x)$ and $\phi_1(x) = \widetilde{\sigma}_{\phi_1}^{-1}\varphi_1(\widetilde{\sigma}_{\phi_1}^{-1}x)$ Under the changes of variables $y = x - \sigma_\phi z$ and $y = x - \widetilde{\sigma}_{\phi_1} z$, respectively, $P_T \boldsymbol{v} = ((P_T \boldsymbol{v})_1, (P_T \boldsymbol{v})_2)$ satisfies

$$T\,(P_T \boldsymbol{v})_1 = u(x,t+T) - C\int_{-\infty}^{\infty} \varphi(z) f\left(u\left(x-\sigma_\phi z,t\right), w\left(x-\sigma_\phi z,t\right)\right) \mathrm{d}z, \tag{10a}$$

$$T\,(P_T \boldsymbol{v})_2 = w(x,t+T) - D\int_{-\infty}^{\infty} \varphi_1(z) g\left(u\left(x-\widetilde{\sigma}_{\phi_1} z,t\right), w\left(x-\widetilde{\sigma}_{\phi_1} z,t\right)\right) \mathrm{d}z. \tag{10b}$$

Due to the parameter setting (6), small values of T correspond to small values of σ_ϕ and $\widetilde{\sigma}_{\phi_1}$ Hence, to investigate the system's behaviour for $T \ll 1$, consider the Taylor expansions of $u(x-\sigma_\phi z,t)$, $w(x-\sigma_\phi z,t)$, $u(x-\widetilde{\sigma}_{\phi_1} z,t)$ and $w(x-\widetilde{\sigma}_{\phi_1} z,t)$ about x, which give

$$\begin{aligned}
&f\left(u\left(x-\sigma_\phi z,t\right), w\left(x-\sigma_\phi z,t\right)\right)\\
&\quad = u(x,t)^2 w(x,t) + \left(\frac{1}{C} - B\right) u(x,t)\\
&\qquad - \sigma_\phi z\left(u(x,t)^2 w_x(x,t) + \left(\frac{1}{C} - B\right) u_x(x,t) + 2u(x,t)u_x(x,t)w(x,t)\right)\\
&\qquad + \sigma_\phi^2 z^2\left(\frac{1}{2}u(x,t)^2 w_{xx}(x,t) + u_x(x,t)^2 w(x,t) + \frac{1}{2}\left(\frac{1}{C} - B\right) u_{xx}(x,t)\right.\\
&\qquad \left. + u(x,t)u_{xx}(x,t)w(x,t) + 2u(x,t)u_x(x,t)w_x(x,t)\right) + O\left(\sigma_\phi^3\right),
\end{aligned} \tag{11}$$

and similarly

$$
\begin{aligned}
&g\left(u\left(x-\widetilde{\sigma}_{\phi_1}z\right),w\left(x-\widetilde{\sigma}_{\phi_1}z\right)\right)\\
&\quad=A-u(x,t)^2w(x,t)+\left(\frac{1}{D}-1\right)w(x,t)\\
&\qquad-\widetilde{\sigma}_{\phi_1}z\left(-u(x,t)^2w_x(x,t)+\left(\frac{1}{D}-1\right)w_x(x,t)-2u(x,t)u_x(x,t)w(x,t)\right)\\
&\qquad+\widetilde{\sigma}_{\phi_1}^2z^2\left(-u_x(x,t)^2w(x,t)-\frac{1}{2}u(x,t)^2w_{xx}(x,t)+\frac{1}{2}\left(\frac{1}{D}-1\right)w_{xx}(x,t)\right.\\
&\qquad\left.-u(x,t)u_{xx}(x,t)w(x,t)-2u(x,t)u_x(x,t)w_x(x,t)\right)+O\left(\widetilde{\sigma}_{\phi_1}^3\right),
\end{aligned}
\tag{12}
$$

where the subscripts of u and w denote partial differentiation. Substitution of this into (10) and term-wise integration using Watson's Lemma [e.g. (Miller 2006)] gives

$$
\begin{aligned}
&T\left(P_T\boldsymbol{v}\right)_1=u(x,t+T)-C\left(u(x,t)^2w(x,t)+\left(\frac{1}{C}-B\right)u(x,t)\right.\\
&\quad+\left(u(x,t)^2w_{xx}(x,t)+2(u_x(x,t))^2w(x,t)+\left(\frac{1}{C}-B\right)u_{xx}(x,t)\right.\\
&\quad\left.\left.+2u(x,t)u_{xx}(x,t)w(x,t)+4u(x,t)u_x(x,t)w_x(x,t)\right)\sigma_\phi^2\int_{-\infty}^{\infty}\varphi(z)z^2\mathrm{d}z+O\left(\sigma_\phi^3\right)\right),
\end{aligned}
$$

and

$$
\begin{aligned}
&T\left(P_T\boldsymbol{v}\right)_2=w(x,t+T)\\
&\quad-D\left(2\left(A-u(x,t)^2w(x,t)+\left(\frac{1}{D}-1\right)w(x,t)\right)\int_{-\infty}^{\infty}\varphi_1(z)\mathrm{d}z\right.\\
&\quad+\left(u(x,t)^2w_x(x,t)-\left(\frac{1}{D}-1\right)w_x(x,t)+2u(x,t)u_x(x,t)w(x,t)\right)\widetilde{\sigma}_{\phi_1}\int_{-\infty}^{\infty}\varphi_1(z)z\mathrm{d}z\\
&\quad+\left(-2(u_x(x,t))^2w(x,t)-u(x,t)^2w_{xx}(x,t)+\left(\frac{1}{D}-1\right)w_{xx}(x,t)\right.\\
&\quad\left.\left.-2u(x,t)u_{xx}(x,t)w(x,t)-4u(x,t)u_x(x,t)w_x(x,t)\right)\frac{\widetilde{\sigma}_{\phi_1}^2}{2}\int_{-\infty}^{\infty}\varphi_1(z)z^2\mathrm{d}z+O\left(\widetilde{\sigma}_{\phi_1}^3\right)\right).
\end{aligned}
$$

Using that $\varphi(x)=\sigma_\phi\phi(\sigma_\phi x)$, $\varphi_1(x)=\widetilde{\sigma}_{\phi_1}\phi_1(\widetilde{\sigma}_{\phi_1}x)$, and the definition of the moments of a probability distribution give

$$
\begin{aligned}
&T\left(P_T\boldsymbol{v}\right)_1=u(x,t+T)-C\left(u(x,t)^2w(x,t)+\left(\frac{1}{C}-B\right)u(x,t)+\frac{\sigma_\phi^2}{2C}u_{xx}(x,t)\right.\\
&\quad+\sigma_\phi^2\left(\frac{1}{2}u(x,t)^2w_{xx}(x,t)+(u_x(x,t))^2w(x,t)-\frac{1}{2}Bu_{xx}(x,t)\right.\\
&\quad\left.\left.+u(x,t)u_{xx}(x,t)w(x,t)+2u(x,t)u_x(x,t)w_x(x,t)\right)+O\left(\sigma_\phi^3\right)\right),
\end{aligned}
$$

and

$$T\,(P_T\boldsymbol{v})_2 = w(x,t+T) - D\left(A - u(x,t)^2 w(x,t) + \left(\frac{1}{D} - 1\right) w(x,t)\right.$$
$$- \frac{\mu_{\phi_1}}{D} w_x(x,t) + \frac{\widetilde{\sigma}^2_{\phi_1}}{2D} w_{xx}(x,t) + \mu_{\phi_1}\left(u(x,t)^2 w_x(x,t) + w_x(x,t)\right.$$
$$\left. + 2u(x,t)u_x(x,t)w(x,t)\right) + \widetilde{\sigma}^2_{\phi_1}\left(-(u_x(x,t))^2 w(x,t) - \frac{1}{2}u(x,t)^2 w_{xx}(x,t)\right.$$
$$\left.\left. - \frac{1}{2} w_{xx}(x,t) - u(x,t)u_{xx}(x,t)w(x,t) - 2u(x,t)u_x(x,t)w_x(x,t)\right) + O\left(\widetilde{\sigma}^3_{\phi_1}\right)\right).$$

Applying (6) yields

$$T\,(P_T\boldsymbol{v})_1 = u(x,t+T)$$
$$- \left(u(x,t) + T\left(u(x,t)^2 w(x,t) - Bu(x,t) + u_{xx}(x,t)\right)\right) + O\left(T^2\right),$$

and

$$T\,(P_T\boldsymbol{v})_2 = w(x,t+T)$$
$$- \left(w(x,t) + T\left(A - u(x,t)^2 w(x,t) - w(x,t) + v w_x(x,t) + d w_{xx}(x,t)\right)\right) + O\left(T^2\right),$$

which shows (9).

The Taylor expansions $u(x,t+T) = u(x,t) + T u_t(x,t) + O(T^2)$ and $w(x,t+T) = w(x,t) + T w_t(x,t) + O(T^2)$ yield

$$P_T\boldsymbol{v}(x,t) = \frac{\partial \boldsymbol{v}}{\partial t}(x,t) - \Gamma\boldsymbol{v}(x,t) - h_1(\boldsymbol{v}(x,t)) + O\left(T^2\right),$$

and thus

$$P\boldsymbol{v} - P_T\boldsymbol{v} = O\left(T^2\right),$$

which tends to zero as $T \to 0$.

□

3 Linear stability analysis

A common approach to study the onset of spatial patterns in a model is linear stability analysis. Spatial patterns occur if a steady state that is stable to spatially homogeneous perturbations becomes unstable if a spatially heterogeneous perturbation is introduced. In this section we show that such a linear stability analysis of the integrodifference model (5) on flat ground with the Laplacian kernels in the parameter setting (6) yields a condition for pattern onset that is equivalent to the corresponding condition for the local Klausmeier model (1). This implies that pattern onset is independent of the parameter T, the temporal separation of seed dispersal events.

The steady states of (5) are identical with those of the Klausmeier models (1) and (2), i.e.

$$(\overline{u}_1, \overline{w}_1) = (0, A)\,, \quad (\overline{u}_2, \overline{w}_2) = \left(\frac{2B}{A - \sqrt{A^2 - 4B^2}}, \frac{A - \sqrt{A^2 - 4B^2}}{2}\right),$$
$$(\overline{u}_3, \overline{w}_3) = \left(\frac{2B}{A + \sqrt{A^2 - 4B^2}}, \frac{A + \sqrt{A^2 - 4B^2}}{2}\right).$$

Existence of $(\overline{u}_2, \overline{w}_2)$ and $(\overline{u}_3, \overline{w}_3)$ requires $A > A_{\min} := 2B$. The steady states are independent of C, D and the dispersal widths a, a_1 and a_2 and are thus independent of frequency changes to the temporal intermittency when using the scalings (6). For the Klausmeier models $(\overline{u}_1, \overline{w}_1)$ and $(\overline{u}_2, \overline{w}_2)$ are stable to spatially homogeneous perturbations, while $(\overline{u}_3, \overline{w}_3)$ is unstable to spatially homogeneous perturbations in the biologically relevant parameter region $B < 2$ (Klausmeier 1999; Sherratt 2005; Eigentler and Sherratt 2018). Preservation of this structure of the steady states in the integrodifference model (5) is only achieved in a certain parameter region.

Proposition 2 *If*

$$D = \ell\overline{D},\ \ell < 1, \quad C = \frac{\ell_1\overline{D}}{B(m - \ell_1\overline{D})},\ m > 2, \ell_1 < 1, \tag{13}$$

where

$$\overline{D} = \frac{2\left(A^2 - A\sqrt{A^2 - 4B^2} - 2B^2\right)}{A^2 - A\sqrt{A^2 - 4B^2}}, \tag{14}$$

then $(\overline{u}_1, \overline{w}_1)$ *and* $(\overline{u}_2, \overline{w}_2)$ *are stable to spatially homogeneous perturbations, and* $(\overline{u}_3, \overline{w}_3)$ *is unstable to spatially homogeneous perturbations.*

This condition is sufficient but not necessary. Outside this region further restrictions on the rainfall parameter A can be imposed to guarantee conservation of the steady state structure. In the limiting case (6) such a restriction on the rainfall parameter cannot be avoided. The following condition ensures that (13) holds in the limiting case (6).

Corollary 3 *If*

$$A^2 < A_+^2 := \min\left\{\frac{4B^2}{(2 - T)T}, \frac{B(BT + 1)^2}{T}\right\}, \quad T < \frac{1}{2}, \quad B < 2, \tag{15}$$

in (5) *with* $C = D = T$, *then* $(\overline{u}_1, \overline{w}_1)$ *and* $(\overline{u}_2, \overline{w}_2)$ *are stable to spatially homogeneous perturbations, and* $(\overline{u}_3, \overline{w}_3)$ *is unstable to spatially homogeneous perturbations.*

In the limit $T \to 0^+$ this becomes the whole A-B parameter region considered for the continuous-time Klausmeier models, providing a reasonable framework for a comparison of the two models. The upper bounds on T and A do, however, introduce a significant restriction on the model as no arbitrarily large time between dispersal events or large precipitation volumes A can be considered. In this, as well as the parameter region given by (13), the plant density $u_n(x)$ and the water density $w_n(x)$ remain positive for initial conditions close to the steady states. This is sufficient for the linear stability analysis and simulations that follow. In the parameter region in which $(\overline{u}_2, \overline{w}_2)$ is unstable, four different behaviours of the system's solution can be observed; (i) convergence to the desert steady state, (ii) divergence, (iii) a chaotic solution or (iv) a periodic solution for which period doubling occurs as T is increased. However, these different behaviours can yield negative densities of the system's quantities and are thus not considered further in this paper.

Spatial patterns of (5) arise if the steady state $(\overline{u}, \overline{w}) := (\overline{u}_2, \overline{w}_2)$, which is stable to spatially homogeneous perturbations, becomes unstable if a spatially heterogeneous perturbation is introduced.

Proposition 4 *The steady state $(\overline{u}, \overline{w})$ is stable to spatially heterogeneous perturbations if $|\lambda(k)| < 1$ for both eigenvalues of the Jacobian*

$$J = \begin{pmatrix} C\widehat{\phi}(k)\alpha & C\widehat{\phi}(k)\beta \\ D\widehat{\phi_1}(k)\gamma & D\widehat{\phi_1}(k)\delta \end{pmatrix}, \tag{16}$$

for all $k > 0$, where

$$\begin{aligned} \alpha &= f_u(\overline{u}, \overline{w}) = \frac{BC+1}{C}, \\ \beta &= f_w(\overline{u}, \overline{w}) = \frac{4B^2}{\left(A - \sqrt{A^2 - 4B^2}\right)^2}, \quad \gamma = g_u(\overline{u}, \overline{w}) = -2B, \\ \delta &= g_w(\overline{u}, \overline{w}) = -\frac{2\left(A^2 D - AD\sqrt{A^2 - 4B^2} - A^2 + A\sqrt{A^2 - 4B^2} + 2B^2\right)}{D\left(A - \sqrt{A^2 - 4B^2}\right)^2}. \end{aligned} \tag{17}$$

Due to the asymmetry of ϕ_1 some of the entries of the Jacobian (16) are complex-valued. A significant simplification can therefore be achieved by considering the integrodifference model (5) on flat ground. This corresponds to $a_1 = 0$ in ϕ_1. As a consequence, the Jury conditions [see e.g. Murray (1989)] can be used to determine the steady state's stability to spatially heterogeneous perturbations. To study this in more detail, and in particular to show that the model does not provide information on effects the temporal separation of seed dispersal events, we focus on the limiting case (6) and the Laplacian kernel (3).

Proposition 5 *The steady state $(\overline{u}, \overline{w})$ of the integrodifference model (5) under the scalings (6) on flat ground with the Laplacian kernels (3) is unstable to spatially*

heterogeneous perturbations if

$$1 + \det(J) - |\mathrm{tr}(J)| < 0, \quad \textit{for some } k > 0, \tag{18}$$

where J is the Jacobian given in Proposition 4 with $a_1 = 0$.

In other words, Proposition 5 provides a sufficient condition for spatial patterns to occur. The following proposition shows that (18) is equivalent to the stability condition (4) of $(\overline{u}, \overline{w})$ in the local Klausmeier model. In other words, a diffusion driven instability causes the occurrence of spatial patterns in the integrodifference model, i.e. given a level of rainfall A, an instability occurs for $d > d_c(A, B)$, where $d_c(A, B)$ is given in (4).

Proposition 6 *The steady state $(\overline{u}, \overline{w})$ of the integrodifference model (5) under the scalings (6) on flat ground with the Laplacian kernels (3) is unstable to spatially heterogeneous perturbations if $d > d_c(A, B)$, where the threshold d_c is identical with the corresponding threshold (4) for the local Klausmeier model.*

The condition's independence of T yields that the integrodifference model does not provide any information on the effects of the temporal separation of seed dispersal events on the onset of spatial patterns. The equivalence of the condition to that of the local Klausmeier model follows directly from the condition's independence of T and Proposition 1, which shows that the integrodifference model converges to the local Klausmeier model as $T \to 0^+$. Thus for sufficiently small values of T, Proposition 6 does indeed provide the exact same information as the diffusion threshold obtained for the local Klausmeier model. For larger T the model does not provide any information on the transition between uniform and patterned vegetation as the decrease in the upper bound A_+ on the rainfall parameter reduces the size of the rainfall interval for which the derivation of d_c is valid.

Proof of Proposition 2 Stability of a steady state $(\overline{u}, \overline{w})$ is determined by the Jury conditions applied to the Jacobian

$$J = \begin{pmatrix} C(2\overline{u}\,\overline{w} - B) + 1 & C\overline{u}^2 \\ -2D\overline{u}\,\overline{w} & -D(\overline{u}^2 + 1) + 1 \end{pmatrix}.$$

The steady state $(\overline{u}_3, \overline{w}_3)$ is unstable in the whole parameter region, because

$$1 + \det(J) - |\mathrm{tr}(J)| = -\frac{2BCD\left(A^2 + A\sqrt{A^2 - 4B^2} - 4B^2\right)}{\left(A + \sqrt{A^2 - 4B^2}\right)^2} < 0.$$

The desert steady state $(\overline{u}_1, \overline{w}_1)$ is monotonically stable if $C < B^{-1}$ and $D < 1$. If $1 < D < 2$ or $B^{-1} < C < 2B^{-1}$ it is still stable but solutions are oscillating about $(0, A)$, which is biologically impossible. Finally, the Jury conditions yield that

$(\overline{u}_2, \overline{w}_2)$ is stable to spatially homogeneous perturbations if $\min\{\overline{C_2}, \overline{C_3}\} < C < \overline{C_1}$, where

$$\overline{C_1} = \frac{AD\left(A - \sqrt{A^2 - 4B^2}\right)}{B\left((D-1)A\left(\sqrt{A^2-4B^2} - A\right) + 2B^2(2D-1)\right)},$$

$$\overline{C_2} = \frac{2\left((D-2)\left(A\sqrt{A^2-4B^2} - A^2\right) - 4B^2\right)}{B\left((D-2)\left(A^2 - A\sqrt{A^2-4B^2}\right) - 4B^2(D-1)\right)},$$

$$\overline{C_3} = \frac{(D-2)\left(A^2 - A\sqrt{A^2-4B^2}\right) + 4B^2}{B\left(A^2 - A\sqrt{A^2-4B^2} - 2B^2\right)}.$$

Combined, this gives that the steady state structure of the continuous time model is preserved if

$$D < 1 \quad \text{and} \quad \max\left\{0, \min\left\{\overline{C_2}, \overline{C_3}\right\}\right\} < C < \min\left\{\frac{1}{B}, \overline{C_1}\right\}. \tag{19}$$

If $D > 1/2$, then $\min\left\{1/B, \overline{C_1}\right\} = 1/B$, because

$$\overline{C_1} - \frac{1}{B} = -\frac{2\left(D - \frac{1}{2}\right)\left(A^2 - A\sqrt{A^2-4B^2} - 2B^2\right)}{B\left(\left(D-\frac{1}{2}\right)\left(A^2 - A\sqrt{A^2-4B^2} - 4B^2\right) - \left(A^2 - A\sqrt{A^2-4B^2}\right)\right)} > 0,$$

since $A^2 - A\sqrt{A^2-4B^2} - 2B^2 > 0$ and $A^2 - A\sqrt{A^2-4B^2} - 4B^2 < 0$. Similarly, if $D < 1/2$, then $\min\left\{1/B, \overline{C_1}\right\} = \overline{C_1}$. Further, if $D < \overline{D}$ (defined in (14)), then $\max\{0, \min\{\overline{C_2}, \overline{C_3}\}\} = 0$ and similarly, if $D > \overline{D}$, then $\max\{0, \min\{\overline{C_2}, \overline{C_3}\}\} = \overline{C_2}$.

Hence, (19) can be simplified by splitting it into different parameter regions. It becomes (i) $C < \overline{C_1}$ if $D < 1/2$ and $D < \overline{D}$, (ii) $\overline{C_2} < C < \overline{C_1}$ if $D < 1/2$ and $\overline{D} < D < 1$, (iii) $C < 1/B$ if $1/2 < D < 1$ and $D < \overline{D}$ and (iv) $\overline{C_2} < C < 1/B$ if $1/2 < D < 1$ and $\overline{D} < D < 1$.

This classification is used below to show that if C and D are defined as in (13), then (19) is satisfied in the whole parameter plane that is considered in the continuous-time PDE models ($A > 2B$, $B < 2$). To show this it is sufficient to show that (i) and (iii) are satisfied because $\ell < 1$. For case (iii) note that

$$C = \frac{\ell_1 D}{B(m - \ell_1 D)} < \frac{1}{B} \iff \ell_1 D < \frac{m}{2},$$

which is satisfied since $\ell_1 D < 1$ and $m > 2$. For case (i) note that

$$C = \frac{\ell_1 D}{B(m - \ell_1 D)} < \overline{C_1} \iff \ell_1 D < \frac{2B^2 + (m-1)\left(A^2 - A\sqrt{A^2+4B^2}\right)}{4B^2} := \overline{\overline{D}}.$$

This is always satisfied because $\ell_1 D < 1$ and

$$\overline{\overline{D}} > 1 \iff m > \frac{2B^2}{A^2 - A\sqrt{A^2 + 4B^2}} + 1 := \overline{m},$$

which holds true since $m > 2$ and

$$\overline{m} < 2 \iff A^2 - A\sqrt{A^2 - 2B^2} - 2B^2 > 0,$$

which is clearly satisfied.

□

Proof of Proposition 4 Linearisation of the model (5) about the steady state $(\overline{u}, \overline{w})$ gives $u_{n+1}(x) = C\phi(\cdot) * (\alpha u_n(\cdot) + \beta w_n(\cdot))$ and $w_{n+1}(x) = D\phi_1(\cdot) * (\gamma u_n(\cdot) + \delta w_n(\cdot))$. Taking the Fourier transform of both equations yields $\widehat{u}_{n+1}(k) = C\widehat{\phi}(k)(\alpha\widehat{u}_n(k) + \beta\widehat{w}_n(k))$ and $\widehat{w}_{n+1}(k) = D\widehat{\phi_1}(k)(\gamma\widehat{u}_n(k) + \delta\widehat{w}_n(k))$, where $\widehat{\phi}$ and $\widehat{\phi_1}$ denote the Fourier transforms of the kernels ϕ, and ϕ_1, respectively. Under the assumption that $\widehat{u}_n(k)$ and $\widehat{w}_n(k)$ are proportional to $\lambda^n\tilde{u}(k)$ and $\lambda^n\tilde{w}(k)$, respectively, where $\lambda \in \mathbb{C}$ denotes the growth rate, the system becomes $\lambda\tilde{u}(k) = C\widehat{\phi}(k)(\alpha\tilde{u}(k) + \beta\tilde{w}(k))$ and $\lambda\tilde{w}(k) = D\widehat{\phi_1}(k)(\gamma\tilde{u}(k) + \delta\tilde{w}(k))$, i.e. λ is an eigenvalue of the Jacobian J. □

Proof of Proposition 5 For an instability to occur, at least on of the Jury conditions $\det(J) < 1$ and $1 + \det(J) - |\mathrm{tr}(J)| > 0$ needs to be violated for some wavenumber $k > 0$. The former condition is satisfied for all $k > 0$. To show this, note that that $\max\{\det(J) - 1\}$ is at $k = 0$ because

$$\det(J) - 1 = \frac{\alpha_4 k^4 + \alpha_2 k^2 + \alpha_0}{\left(dTk^2 + 1\right)\left(A - \sqrt{A^2 - 4B^2}\right)^2\left(Tk^2 + 1\right)}, \tag{20}$$

where

$$\begin{aligned}
\alpha_4 &= 2dT^2\left(-A^2 + A\sqrt{A^2 - 4B^2} + 2B^2\right),\\
\alpha_2 &= -2T\left(A^2 - A\sqrt{A^2 - 4B^2} - 2B^2\right)(d + 1),\\
\alpha_0 &= 2T\left(\left(\frac{1}{2}B - 1\right)\left(A^2 - A\sqrt{A^2 - 4B^2}\right)\right.\\
&\quad \left. + \left(\frac{1}{2}B - TB\right)\left(A^2 - A\sqrt{A^2 - 4B^2} - 4B^2\right)\right).
\end{aligned}$$

The denominator of (20) is clearly positive and increasing for $k > 0$. Since further $\alpha_4 < 0$ and $\alpha_2 < 0$, the numerator and thus the whole of (20) is decreasing for $k > 0$ and it attains its maximum at $k = 0$. The negativity of (20) then follows from that of α_0 which follows from $B < 2$ and $T < 1/2$.

□

Proof of Proposition 6 Firstly, we note that $\partial d_c/\partial A \geq 0$ for all $A \geq 2B$. Hence, d_c attains its minimum on $A = 2B$, on which it simplifies to $d_c = 2/B$. Since $B < 2$, $d_c > 1$. Next, we show that $\mathrm{tr}(J) > 0$. To do this, note that

$$\mathrm{tr}(J) = \frac{\beta_2 k^2 + \beta_0}{\left(dTk^2+1\right)\left(A-\sqrt{A^2-4B^2}\right)^2\left(Tk^2+1\right)} > 0,$$

for all $k > 0$, where

$$\beta_2 = 2\left(A^2 - A\sqrt{A^2-4B^2} - 2B^2\right)\left(BT^2d + T + Td\right) - 2T^2\left(A^2 - A\sqrt{A^2-4B^2}\right),$$
$$\beta_0 = 2\left(BT - T + 2\right)\left(A^2 - A\sqrt{A^2-4B^2} - 2B^2\right).$$

The denominator is clearly positive and thus the condition for positivity of $\mathrm{tr}(J)$ is $\beta_2 k^2 + \beta_0 > 0$. The left hand side of this is decreasing in A since $A^2 - A\sqrt{A^2-4B^2}$ is decreasing in A and the assumptions on B and d, and thus obtains its minimum at $A = A^+$, where A^+ is given in (15). If $B < 1/(2-T)$, then $A^+ = 4B^2/((2-T)T)$ and

$$\mathrm{tr}(J)\left(\sqrt{A^+}\right) > 0 \Longleftrightarrow k^2 > \frac{B}{1-d-BTd},$$

since $d > 1$. The right hand side is negative and thus $\min(\mathrm{tr}(J)) > 0$ for $B < 1/(2-T)$. If $B > 1/(2-T)$, then $A^+ = (BT+1)^2B/T$ and

$$\mathrm{tr}(J)\left(\sqrt{A^+}\right) > 0 \Longleftrightarrow k^2 > -\frac{TB^2 + (2-T)B - 1}{B^2T^2d + \left((d+1)T - T^2\right)B - T},$$

since $d > 1$. Negativity of the right hand side follows from the lower bound on B and thus $\min(\mathrm{tr}(J)) > 0$ for all $B < 2$. This shows that $\mathrm{tr}(J) > 0$. The stability condition (18) thus becomes $1 + \det(J) - \mathrm{tr}(J) < 0 \Longleftrightarrow \gamma_4 k^4 + \gamma_2 k^2 + \gamma_0 < 0$, where $\gamma_4 = d(A^2 - A\sqrt{A^2-4B^2} - 2B^2)$, $\gamma_2 = (A^2 - A\sqrt{A^2-4B^2})(1-Bd) + 2B^3d$ and $\gamma_0 = B(A^2-4B^2)$. This condition and thus its minimum $-\gamma_2^2/(4\gamma_4) + \gamma_0$ is independent of T. Determining the locus at which the minimum changes sign gives the threshold $d_c(A, B)$. □

4 Simulations

The preceding linear stability analysis relies on the use of the Laplace kernel. For other kernel functions whose Fourier transforms do not provide such a simplification numerical simulations of the model are considered to investigate the onset of patterns. In particular, this allows us to make comparisons between different dispersal kernels, similar to the analysis performed for the nonlocal model in Eigentler and Sherratt (2018). These show that both wide plant dispersal kernels and narrow water dispersal kernels inhibit the formation of patterns. Finally in this section, we show that as for the

nonlocal Klausmeier model, the kind of decay of the plant dispersal kernel at infinity is also important.

Simulations are performed on the space domain $[-x_{\max}, x_{\max}]$ centred at $x = 0$. This domain is discretised into M equidistant points $x_1, \dots, x_M$ with $-x_{\max} = x_1 < x_2 < \cdots < x_M = x_{\max}$ such that $\Delta x = x_2 - x_1 = \cdots = x_M - x_{M-1}$. On flat ground (5) then becomes

$$u_{n+1}(x_k) = C\Delta x\,(\phi * f_n)_k\,, \tag{21a}$$

$$w_{n+1}(x_k) = D\Delta x\,(\phi_1 * g_n)_k\,, \tag{21b}$$

where ϕ, ϕ_1 denote the vectors consisting of the elements obtained by evaluating the corresponding function at each mesh point, f_n, g_n denote the vectors consisting of the elements obtained by evaluating the corresponding function at each $(u_n(x_k), w_n(x_k))$ and $z_1 * z_2$ denotes the discrete convolution of two vectors z_1 and z_2. The convolution terms in (21a) and (21b) are obtained by using the convolution theorem and the fast Fourier transform, providing a significant simplification as this reduces the number of operations required to obtain the convolution from $O(M^2)$ to $O(M\log(M))$ [see e.g. Cooley et al. (1969)].

To mimic the infinite domain used for the linear stability analysis (Sect. 3), we define the initial condition of the system as follows; on a subdomain $[-x_{\text{sub}}, x_{\text{sub}}]$ centred at $x = 0$ of the domain $[-x_{\max}, x_{\max}]$ considered in the simulation the initial condition is a random perturbation of the steady state $(\overline{u}, \overline{w})$, while on the rest of the domain the densities are initially set to equal the densities of the steady state $(\overline{u}, \overline{w})$. In other words, $u_0(x_k) = \overline{u} + \delta(x_k)$ and $w_0(x_k) = \overline{w} + \varepsilon(x_k)$ for $x_k \in [-x_{\text{sub}}, x_{\text{sub}}]$, where $\|\delta\|_\infty < 0.1\overline{u}$ and $\|\varepsilon\|_\infty < 0.1\overline{w}$ and $u_0(x_k) = \overline{u}$ and $w_0(x_k) = \overline{w}$ for $x_k \notin [-x_{\text{sub}}, x_{\text{sub}}]$. The size of the outer domain is chosen large enough so that any boundary conditions (which are set to be periodic) that are imposed on $[-x_{\max}, x_{\max}]$ do not affect the solution in the subdomain in the finite time that is considered in the simulation. Figure 1 shows a typical patterned solution obtained by these simulations.

Based on the amplitude of the oscillation relative to the steady state of the solutions obtained by the simulations we set up a scheme to determine the critical rainfall level $A_{\max}$ below which pattern onset occurs. Doing this allows us to investigate how certain changes of parameters and kernel functions affect the onset of patterns. Due to the random perturbation of the initial state of the system, all simulation results shown below are the averages taken over 100 simulations. For the symmetric dispersal kernels ϕ and ϕ_1 we consider the Laplacian (3), the Gaussian

$$\phi_g(x) = \frac{a_g}{\sqrt{\pi}} e^{-a_g^2 x^2}, \quad a > 0, x \in \mathbb{R}, \tag{22}$$

and the power law distribution

$$\phi_p(x) = \frac{(b-1)a_p}{2\left(1 + a_p|x|\right)^b}, \quad a > 0, b > 3, x \in \mathbb{R}. \tag{23}$$

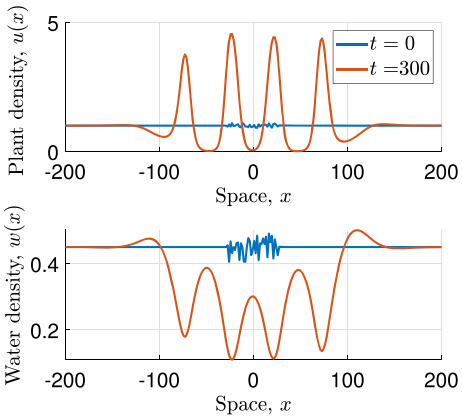

Fig. 1 Simulation of the integrodifference model. This figure shows a patterned solution obtained by simulating the integrodifference model on flat ground. The kernels used in these simulations are the symmetric Laplacian kernels, respectively. The parameter setting (15) with $T = 0.1$ is used in the simulation. The other parameters are $A = 0.9$, $B = 0.45$ and $d = 500$

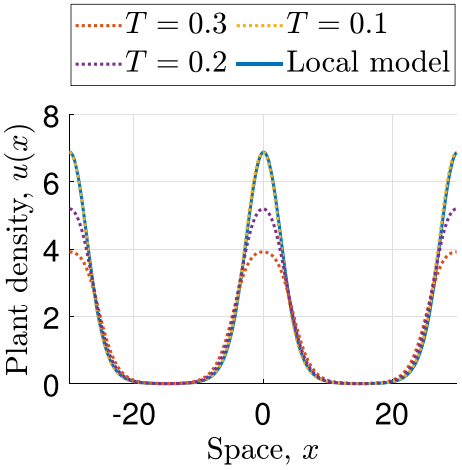

Fig. 2 Convergence of solutions. This figure visualises the convergence of solutions to the local PDE model (1) as $T \to 0^+$, to complement the consistency result presented in Proposition 1. Solutions of the integrodifference model (5) are shown for $T = 0.3$, $T = 0.2$ and $T = 0.1$ and are compared with the solution of the local Klausmeier PDE model (1). Note that unlike in Fig. 1, the spatial domain is chosen to be small to impose the same wavelength restrictions on both models to aid the visualisation of the convergence

We base our comparison on the kernels' standard deviations, which are given by $\sigma_\phi = \sqrt{2}/a$ for the Laplacian kernel (3), $\sigma_{\phi_g} = 1/(\sqrt{2}\, a_g)$ for the Gaussian kernel (22) and $\sigma_{\phi_p} = \sqrt{2}/(\sqrt{b^2 - 5b + 6}\, a_p)$ for the power law kernel (23) provided $b > 3$. It is perfectly reasonable to perform simulations with kernels of infinite standard deviation (e.g. $b < 3$ in the power law kernel) but in the interest of comparing results for the kernels based on their standard deviation we consider only $b = 3.1$ and $b = 4$.

To investigate the model's behaviour under changes to the dispersal kernels ϕ and ϕ_1, we start by considering simultaneous changes in the kernel functions ϕ, and ϕ_1. The comparison between the kernel functions is based on the standard deviation of the plant dispersal kernel ϕ and the width of the water dispersal kernel ϕ_1 is set to $a_2 = 0.1a$ to obtain a ratio similar to that of the standard deviations under the scalings (6), which corresponds to the large value of the diffusion parameter d in the PDE and integro-PDE models. Figure 3 visualises the simulation results, which show that for small standard deviations, the rainfall threshold $A_{\max}$ is close to its lower bound, before an increase in the kernel width causes it to peak before slowly decreasing as the

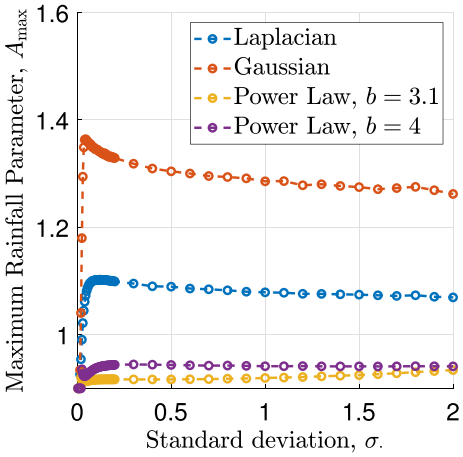

Fig. 3 The maximum rainfall parameter $A_{\max}$ under simultaneous changes of the dispersal kernels. This figure visualises variations of $A_{\max}$ against simultaneous variations of both kernel functions. The standard deviation on the abscissa refers to the plant dispersal kernel ϕ, the width of the water dispersal kernel ϕ_1 is set to $a_2 = 0.1a$. The rainfall threshold is determined up to an interval of length 10^{-4} for $\sigma_\phi = \{0.01, 0.02, \ldots, 0.05, 0.1, 0.2, \ldots, 2\}$. The parameter values used for this simulation are $B = 0.45$, $\ell = \ell_1 = 0.5$, $m = 5$

kernel widths are further increased. For very narrow dispersal kernels very little spatial interaction takes place. In particular, as $\sigma \to 0$, the kernel functions tend to the delta function $\delta(x)$ centred at 0 and therefore the integrodifference system (5) becomes

$$u_{n+1}(x) = u_n(x) + C\left(u_n(x)^2 w_n(x) - B u_n(x)\right),$$
$$w_{n+1}(x) = w_n(x) + D\left(A - u_n(x)^2 w_n(x) - w_n(x)\right).$$

For this system, the steady state $(\overline{u_2}, \overline{w_2})$, which was randomly perturbed to set the initial condition of the system in the simulation, is always stable. Therefore, no patterns exist and $A_{\max} = 2B$ is the minimum value of the rainfall parameter for which vegetation is growing uniformly, recalling that for $A < 2B$, the steady state $(\overline{u_2}, \overline{w_2})$ does not exist. Further, away from $\sigma = 0$, a change in kernel width only has very little effect on $A_{\max}$, an indication that an increase to the width of the plant dispersal kernel has the opposite effect on the tendency to form patterns as an increase to the width of the water dispersal kernel.

To test this hypothesis, we investigate changes in the system's behaviour as individual kernel functions are changed. First, we consider how the critical rainfall parameter $A_{\max}$ is affected by a change of the shape of the dispersal kernel ϕ in the plant equation (21a). The result (see Fig. 4a) is consistent with results of the integro-PDE model (Eigentler and Sherratt 2018) on sloped ground. Firstly, an increase in the width of the plant dispersal kernels reduces the size of the parameter region supporting pattern onset, where changes for larger values of the standard deviation σ_ϕ are much smaller than close to $\sigma_\phi = 0$. Identical to the nonlocal Klausmeier model, a trend that for small standard deviations those kernel functions that decay algebraically at infinity predict a lower value of $A_{\max}$ than those decaying exponentially, and vice versa for larger kernel widths, is also observed in these simulations.

Next, we perform a similar analysis for the symmetric water dispersal kernel ϕ_1. To be consistent with the setting $a_2 = 0.1a$ in the simulation for the simultaneous change of the kernel functions, we consider a larger range of σ_{ϕ_1} for this simulation. The

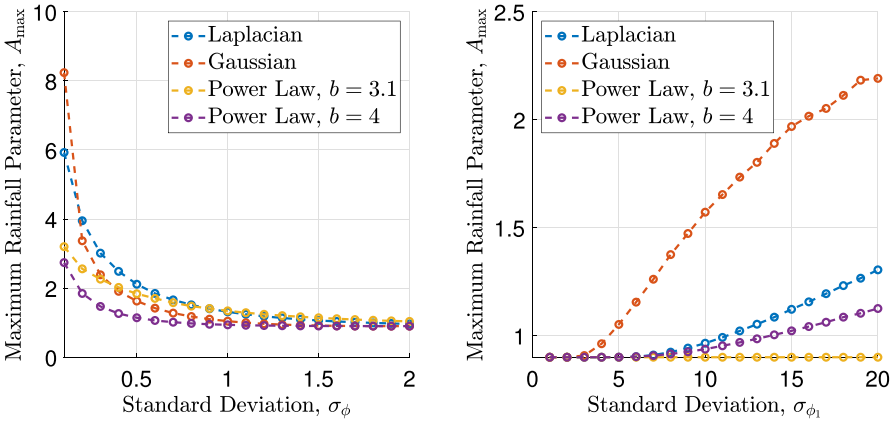

(a) Changes to plant dispersal kernel only **(b)**Changes to water dispersal kernel only

Fig. 4 The maximum rainfall parameter $A_{\max}$ under separate variations of the dispersal kernels. **a** $A_{\max}$ up to an interval of length 10^{-4} with varying width ($\sigma_\phi = \{0.05, 0.1, 0.2, \ldots, 2\}$) and shape of the plant dispersal kernel ϕ, while **b** visualises the effects of changes in the water dispersal kernel ϕ_1. The latter was simulated for a larger range of the kernel's standard deviation σ_{ϕ_1}, specifically $\sigma_{\phi_1} = \{1, 2, \ldots, 20\}$, to account for the choice of $a_2 = 0.1a$ in the previous simulation. Also in (b) $A_{\max}$ is determined up to an interval of length 10^{-4}. The widths of the fixed kernels are set to $a_2 = 0.1$ (**a**) and $a = 1$ (**b**), respectively. The other parameter values used both simulations are $B = 0.45$, $\ell = \ell_1 = 0.5$, $m = 5$

results (Fig. 4b) show that for narrow kernels, $A_{\max}$ is close to its minimum $A = 2B$, i.e. the rainfall interval supporting pattern formation is very small. In particular, as $\sigma_{\phi_1} \to 0$, $A_{\max} \to 2B$ and no patterns can occur. For the Laplace kernel, this can also be shown using linear stability analysis. If $\sigma_{\phi_1} = 0$, then $\widehat{\phi_1} \equiv 1$ and thus the Jacobian (16) becomes

$$J = \begin{pmatrix} C\widehat{\phi}(k)\alpha & C\widehat{\phi}(k)\beta \\ D\gamma & D\delta \end{pmatrix}.$$

Further, the stability condition is

$$k^2 > \frac{BCa^2\left(A^2 - A\sqrt{A^2 - 4B^2} - 4B^2\right)}{A^2 - A\sqrt{A^2 - 4B^2}}.$$

The right hand side is negative and thus the steady state is always stable to spatially heterogeneous perturbations. An increase of the kernel width then causes an increase in the rainfall threshold $A_{\max}$, where those kernels that decay exponentially at infinity, yield a larger increase than those decaying algebraically.

The results above confirm that the plant dispersal kernel ϕ and the water dispersal kernel ϕ_1 have opposite effects on the rainfall threshold $A_{\max}$. While an increase in the width of the plant dispersal inhibits the onset of patterns, an increase in the standard deviation of the water dispersal kernel increases the tendency to form patterns. This explains the nearly constant value of $A_{\max}$ in the simulations in which both kernel

functions are varied simultaneously. Consequently, these results suggest that it is the ratio of plant dispersal to water dispersal, i.e. the ratio $\sigma_\phi/\sigma_{\phi_1}$ that controls the tendency to form patterns. An increase in the ratio inhibits the onset of patterns, while a decrease has the opposite effect.

5 Discussion

The deliberately basic description of the plant–water dynamics in semi-arid environments by the Klausmeier model provides a rich framework for model extensions to address a range of different features of dryland ecosystems and their effects on vegetation patterns. Extensions include cross advection due to decreased surface water run-off resulting from an increase in infiltration in biomass patches (Wang and Zhang 2019); terrain curvature (Gandhi et al. 2018); nonlocal dispersal of seeds (Eigentler and Sherratt 2018; Bennett and Sherratt 2018); secondary seed dispersal due to overland water flow (Consolo and Valenti 2019); nonlocal grazing effects (Siero et al. 2019; Siero 2018); explicit modelling of a population of grazers (Fernandez-Oto et al. 2019); local competition between plants (Wang and Zhang 2018); the inclusion of autotoxicity (Marasco et al. 2014); multispecies plant communities (Eigentler and Sherratt 2019; Ursino and Callegaro 2016; Callegaro and Ursino 2018) and seasonality and intermittency in precipitation (Ursino and Contarini 2006; Eigentler and Sherratt 2020). One aspect that has not yet been considered in this context is the seasonal separation of plant growth and seed dispersal. In this paper we have considered the synchronised and seasonal occurrence of nonlocal seed dispersal through a system of integrodifference equations based on the Klausmeier reaction-advection-diffusion system.

While an integrodifference system cannot explicitly quantify the temporal separation of seed dispersal occurrences, the model's derivation and an associated convergence result (Proposition 1) yield a parameter setting in which the length of the growth phase between dispersal stages can be accounted for. However, the main result of the linear stability analysis of the integrodifference model in this paper (Proposition 6) shows that conditions for pattern onset in the integrodifference model (5) are independent of the temporal separation of seed dispersal from plant growth. Moreover, due to the model's derivation form the Klausmeier model (1), the pattern onset conditions for both models are equivalent.

Some semi-arid environments in which vegetation patterning is a common phenomenon are characterised by large temporal and in particular seasonal fluctuations in their environmental conditions (Noy-Meir 1973; Chesson et al. 2004). For example, observed patterns in Spain, Israel and North America are all located in Mediterranean climate zones (Peel et al. 2007), in which precipitation mainly occurs during winter, while during the summer months little or no rainfall occurs. By contrast, most mathematical models describing these ecosystems employ partial differential equations. While PDE models provide a rich framework for mathematical model analysis, their use is based on the simplifying assumption that all processes occur continuously in time. The results presented in this paper emphasise the importance and significance of results obtained from such models. In the context of seed dispersal, the biologically more realistic temporal separation of plant growth and seed dispersal has no effect on

the conditions for pattern onset to occur. We thus conclude that the results obtained for the Klausmeier PDE model are robust to changes in the temporal properties of seed dispersal processes and that the assumption of continuous seed dispersal provides a sufficiently accurate description.

The parameter setting used to establish a connection between the Klausmeier model (1) and the integrodifference model (5) couples the scale parameter a of the seed dispersal kernel to other model parameters. If, however, a more general parameter setting is considered, then the effects of changes to the average seed dispersal distance and the shape of the seed dispersal kernel can be analysed numerically. Our results, which are in full agreement with an earlier investigation of the nonlocal Klausmeier model (2) (Eigentler and Sherratt 2018), show that seed dispersal over longer distances inhibits the formation of patterns (Fig. 4a). Indeed, the threshold $A_{\max}$ on the rainfall parameter above which no pattern onset occurs, tends to $A_{\min}$, the minimum rainfall level required for the existence of a nontrival spatially uniform equilibrium, as dispersal distances become sufficiently large. Nevertheless, many plant species in semi-arid ecosystems have developed antitelechoric mechanisms which inhibit long range seed dispersal (Ellner and Shmida 1981; van Rheede van Oudtshoorn and van Rooyen 2013). While in the context of this paper this may appear as an evolutionary disadvantage, the development of narrow seed dispersal kernels is a side effect of other adaptations such as the development of seed containers as a protection to predation (Ellner and Shmida 1981). This suggests the existence of an evolutionary trade-off between seed dispersal distance and plant mortality. A numerical study of the threshold $A_{\max}$ in the σ_ϕ-B parameter plane (Fig. 5) gives some useful insight into this. The trade-off would restrict parameters to some increasing curve in the σ_ϕ-B parameter plane. Depending on the exact functional form of such a trade-off, a decrease in the seed dispersal distance σ_ϕ may cause a reduction in the precipitation threshold $A_{\max}$, if the trade-off implies a sufficiently large simultaneous decrease in the plant mortality rate B. A lower $A_{\max}$ value corresponds to an inhibition of pattern onset. We thus conclude that our model can capture the evolutionary advantage associated with the development of protective antitelechoric mechanisms if the trade-off between seed dispersal distance σ_ϕ and plant mortality B is chosen appropriately, but emphasise that we are not aware of any data that provides quantitative information on the exact form of this trade-off.

Our results further indicate that the shape of the seed dispersal kernel, and in particular its decay at infinity, has a significant effect on the onset of patterns. Fat-tailed kernels, for example, that account for a higher proportion of long-range dispersal events, yield a lower level of $A_{\max}$ than kernel functions with exponential decay at infinity for a sufficiently small fixed standard deviation. This highlights the importance of obtaining knowledge of seed dispersal behaviour of plant species, a property that depends on both species and the environment (e.g. seed dispersal agent) (Bullock et al. 2017).

In our integrodifference model (5), we model the redistribution of water through a convolution similar to the modelling of the seed dispersal process. This nonlocal description can account for overland water flow from bare ground to biomass patches across larger distances during precipitation events. It does, however, rely on the assumption that the soil's properties enhance overland water flow in regions of

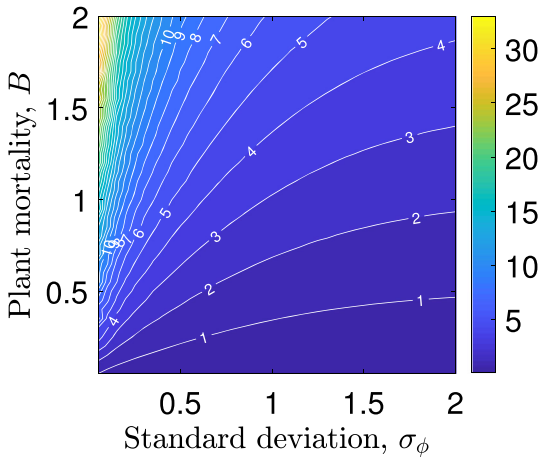

Fig. 5 The threshold $A_{\max}$ in the σ_ϕ-B parameter plane. The numerically obtained rainfall threshold $A_{\max}$ is shown in the σ_ϕ-B parameter plane as a contour plot, where σ_ϕ denotes the standard deviation of the plant dispersal kernel ϕ. It was obtained on the spatial grid $\{0.05, 0.1, \ldots, 1.95, 2\} \times \{0.05, 0.1, \ldots, 1.95, 2\}$ for the Laplace kernel (3) and $a_2 = 0.1$, $\ell = \ell_1 = 0.5$, $m = 5$. We speculate that there may be an evolutionary trade-off between dispersal distance and resistance to predation, which would restrict parameters to an increasing curve in the σ_ϕ-B plane

low biomass. Some ecosystems in semi-arid environments are characterised by soil conditions and soil types (e.g. sand) for which this assumption is invalid (Valentin et al. 1999). The formation of vegetation patterns under such environmental conditions can, however, be explained by other mechanisms, such as laterally extended root networks (Meron 2018). The integrodifference model presented in this paper is based on the assumption that little or no water infiltration occurs in regions of low biomass, and that the overland water flow towards regions of high biomass induced by this soil property is the main mechanism causing the self-organisation into patterns. In this context, our results show that water redistribution over longer distances yields the onset of patterns at higher precipitation levels (Fig. 4b). This is due to the enhancement of the pattern-inducing vegetation-infiltration feedback. Existing biomass patches deplete the water density locally, while regions of bare soil retain a higher water levels. Hence, any redistribution of water has a homogenising effect on the water density which yields to a redistribution of the limiting resource from areas of low biomass to areas of high biomass. An increase in the spatial range of the water redistribution kernel thus strengthens the pattern-inducing feedback and causes pattern onset under larger precipitation volumes.

The work in this paper shows that the description of seed dispersal as a synchronised event during a phase in which no plant growth occurs does not affect the condition for pattern onset compared to the continuous description of seed dispersal in the Klausmeier model (1). The stability of spatial patterns is equally important. A natural area of future work would therefore be an analysis of pattern stability in the integrodifference model (5) comparing results with stability results for the local Klausmeier model (Sherratt and Lord 2007) and the nonlocal Klausmeier model (Bennett and Sherratt 2018). For PDE models, the stability of spatial patterns can be determined through a calculation of their spectra. For this, a method based on numerical continuation has been developed by Rademacher et al. (2007) [for details see Rademacher et al. (2007); Sherratt (2012)]. For integrodifference equations, however, we are not aware of any methods that allow the determination of the stability of a patterned solution.

The integrodifference model (5) not only splits the dynamics of the plant population into separate growth and dispersal stages, but also that of the water dynamics into a water consumption stage and a water redistribution stage. In the model, spatial redistribution of water is synchronised with seed dispersal. This can provide an adequate description for species such as *Mesembryanthemum crystallinum* and *Mesembryanthemum nodiflorum*, which synchronise their seed dispersal with the beginning of the rain season (Navarro et al. 2009), but cannot provide a description of seed dispersal during drought periods or of water flow at any other time during the rain season. While a description of the water flow dynamics during precipitation events in the context of a vegetation model has been proposed by Siteur et al. (2014b), the exact dynamics on flat ground are the subject of ongoing research (e.g. Rossi and Ares 2017; Thompson et al. 2011; Wang et al. 2015) and could be utilised in a future extension of the integrodifference model (5). The description of the water density as one single variable would, however, be prohibitive for such an approach. Instead a distinction between surface water and soil moisture, such as in the Rietkerk et al. model (HilleRisLambers et al. 2001; Rietkerk et al. 2002) or the Gilad et al. model (Gilad et al. 2004), needs to be made to distinguish between surface water flow processes and water uptake processes that take place in the soil.

The integrodifference model (5) and its analysis presented in this paper is restricted to a one-dimensional space domain, motivated by the original formulation of the Klaumeier model and its mathematical accessibility (Klausmeier 1999). However, the consideration of a second space dimension is expected to give more insights into the ecohydroglogical dynamics, in particular on pattern existence and stability. For example, in related PDE models on two-dimensional space domains, different types of patterned solutions exist (gap patterns, labyrinth patterns, striped patterns and gap patterns) and phase transitions along the precipitation gradient can be investigated (Meron 2012). Moreover, even on sloped terrain, the impact of the consideration of a two-dimensional domain is significant, as the analysis on a one-dimensional domain may overestimate the size of the patterns' stability regions (Siero et al. 2015). The analysis of the integrodifference model (5) on a two-dimensional domain presents a considerable challenge, in particular if one would want to obtain a wavenumber-independent results analogous to Proposition 6. Nevertheless, this would be a natural area of potential future work to further disentangle the complex ecosystem dynamics.

Finally, we remark that the integrodifference model (5) describes the discrete structure of plant growth mechanisms caused by the seasonality in precipitation. However, it does not capture the dynamics specific to drought periods between rainfall events and is thus only able to provide an insight into effects of accumulated rainfall volume rather than the temporal separation of precipitation seasons. In separate work, we account for a combination of rainfall, plant growth and seed dispersal pulses with the continuous nature of plant loss and water evaporation and drainage, using an impulsive model (Eigentler and Sherratt 2020). Such models combine partial differential equations with integrodifference equations (see for example Wang and Lutscher (2018) for an impulsive model in the context of predator-prey dynamics with synchronised predator reproduction). The impulsive model has its own limitations as it can only take into account a periodic separation of precipitation events, but not any seasonal patterns. A potential area of future work therefore consists of a combination of these

approaches to describe both the seasonal and intermittent nature of rainfall in semi-arid climate zones.

Acknowledgements Lukas Eigentler was supported by The Maxwell Institute Graduate School in Analysis and its Applications, a Centre for Doctoral Training funded by the UK Engineering and Physical Sciences Research Council (Grant EP/L016508/01), the Scottish Funding Council, Heriot-Watt University and the University of Edinburgh.

References

Bastiaansen R, Jaïbi O, Deblauwe V, Eppinga MB, Siteur K, Siero E, Mermoz S, Bouvet A, Doelman A, Rietkerk M (2018) Multistability of model and real dryland ecosystems through spatial self-organization. Proc Natl Acad Sci. https://doi.org/10.1073/pnas.1804771115

Baudena M, Provenzale A (2008) Rainfall intermittency and vegetation feedbacks in drylands. Hydrol Earth Syst Sci 12:679–689. https://doi.org/10.5194/hess-12-679-2008

Baudena M, Rietkerk M (2013) Complexity and coexistence in a simple spatial model for arid savanna ecosystems. Theor Ecol 6:131–141. https://doi.org/10.1007/s12080-012-0165-1

Bennett JJR, Sherratt JA (2018) Long-distance seed dispersal affects the resilience of banded vegetation patterns in semi-deserts. J Theor Biol 481:151–161. https://doi.org/10.1016/j.jtbi.2018.10.002

Borgogno F, D'Odorico P, Laio F, Ridolfi L (2009) Mathematical models of vegetation pattern formation in ecohydrology. Rev Geophys 47:RG1005. https://doi.org/10.1029/2007RG000256

Bullock JM, González LM, Tamme R, Götzenberger L, White SM, Pärtel M, Hooftman DAP (2017) A synthesis of empirical plant dispersal kernels. J Ecol 105:6–19. https://doi.org/10.1111/1365-2745.12666

Callegaro C, Ursino N (2018) Connectivity of niches of adaptation affects vegetation structure and density in self-organized (dis-connected) vegetation patterns. Land Degrad Dev 29:2589–2594. https://doi.org/10.1002/ldr.2759

Chesson P, Gebauer RLE, Schwinning S, Huntly N, Wiegand K, Ernest MSK, Sher A, Novoplansky A, Weltzin JF (2004) Resource pulses, species interactions, and diversity maintenance in arid and semi-arid environments. Oecologia 141:236–253. https://doi.org/10.1007/s00442-004-1551-1

Clark JS, Lewis M, McLachlan JS, HilleRisLambers J (2003) Estimating population spread: what can we forecast and how well? Ecology 84:1979–1988. https://doi.org/10.1890/01-0618

Consolo G, Valenti G (2019) Secondary seed dispersal in the Klausmeier model of vegetation for sloped semi-arid environments. Ecol Modell 402:66–75. https://doi.org/10.1016/j.ecolmodel.2019.02.009

Consolo G, Currò C, Valenti G (2019) Supercritical and subcritical Turing pattern formation in a hyperbolic vegetation model for flat arid environments. Physica D 398:141–163. https://doi.org/10.1016/j.physd.2019.03.006

Cooley JW, Lewis PAW, Welch PD (1969) The fast Fourier transform and its applications. IEEE Trans Educ 12:27–34. https://doi.org/10.1109/TE.1969.4320436

Cornet A, Delhoume J, Montaña C (1988) Dynamics of striped vegetation patterns and water balance in the Chihuahuan Desert. During H, Werger M. SPB Academic Publishing, Willems H. Diversity and pattern in plant communities. The Hague, pp 221–231

Corrado R, Cherubini AM, Pennetta C (2014) Early warning signals of desertification transitions in semi-arid ecosystems. Phys Rev E Stat Nonlinear Soft Matter Phys 90:062705. https://doi.org/10.1103/PhysRevE.90.062705

Dakos V, Kéfi S, Rietkerk M, van Nes EH, Scheffer M (2011) Slowing down in spatially patterned ecosystems at the brink of collapse. Am Nat 177:E153–E166. https://doi.org/10.1086/659945
Deblauwe V, Couteron P, Bogaert J, Barbier N (2012) Determinants and dynamics of banded vegetation pattern migration in arid climates. Ecol Monogr 82:3–21. https://doi.org/10.1890/11-0362.1
Dickovick JT (2014) Africa 2014–2015. World Today (Stryker). Rowman& Littlefield Publishers, p 374
Eigentler L, Sherratt JA (2020) Effects of precipitation intermittency on vegetation patterns in semi-arid landscapes. Physica D. https://doi.org/10.1016/j.physd.2020.132396
Eigentler L, Sherratt JA (2018) Analysis of a model for banded vegetation patterns in semi-arid environments with nonlocal dispersal. J Math Biol 77:739–763. https://doi.org/10.1007/s00285-018-1233-y
Eigentler L, Sherratt JA (2019) Metastability as a coexistence mechanism in a model for dryland vegetation patterns. Bull Math Biol 81:2290–2322. https://doi.org/10.1007/s11538-019-00606-z
Eldridge D, Zaady E, Shachak M (2000) Infiltration through three contrasting biological soil crusts in patterned landscapes in the Negev, Israel. CATENA 40:323–336. https://doi.org/10.1016/S0341-8162(00)00082-5
Ellner S, Shmida A (1981) Why are adaptations for long-range seed dispersal rare in desert plants? Oecologia 51:133–144. https://doi.org/10.1007/BF00344663
Fernandez-Oto C, Escaff D, Cisternas J (2019) Spiral vegetation patterns in highaltitudewetlands. Ecol Complex 37:38–46. https://doi.org/10.1016/j.ecocom.2018.12.003
Friedman J, Gunderman N, Ellis M (1978) Water response of the hygrochastic skeletons of the true rose of jericho (*Anastatica hierochuntica L.*). Oecologia 32:289–301. https://doi.org/10.1007/BF00345108
Gandhi P, Werner L, Iams S, Gowda K, Silber M (2018) A topographic mechanism for arcing of dryland vegetation bands. J R Soc Interface 15:20180508. https://doi.org/10.1098/rsif.2018.0508
Gilad E, von Hardenberg J, Provenzale A, Shachak M, Meron E (2004) Ecosystem engineers: from pattern formation to habitat creation. Phys Rev Lett 93:098105. https://doi.org/10.1103/PhysRevLett.93.098105
Gowda K, Chen Y, Iams S, Silber M (2016) Assessing the robustness of spatial pattern sequences in a dryland vegetation model. Proc R Soc Lond A 472:20150893. https://doi.org/10.1098/rspa.2015.0893
Gowda K, Iams S, Silber M (2018) Signatures of human impact on self-organized vegetation in the Horn of Africa English. Sci Rep 8:1–8. https://doi.org/10.1038/s41598-018-22075-5
HilleRisLambers R, Rietkerk M, van den Bosch F, Prins HHT, de Kroon H (2001) Vegetation pattern formation in semi-arid grazing systems. Ecology 82:50–61. https://doi.org/10.2307/2680085
Kealy BJ, Wollkind DJ (2012) A nonlinear stability analysis of vegetative Turing pattern formation for an interaction–diffusion plant-surface water model system in an arid flat environment. Bull Math Biol 74:803–833. https://doi.org/10.1007/s11538-011-9688-7
Klausmeier CA (1999) Regular and irregular patterns in semiarid vegetation. Science 284:1826–1828. https://doi.org/10.1126/science.284.5421.1826
Kot M, Schaffer WM (1986) Discrete-time growth-dispersal models. Math Biosci 80:109–136. https://doi.org/10.1016/0025-5564(86)90069-6
Kéfi S, Rietkerk M, Alados CL, Pueyo Y, Papanastasis V, ElAich A, de Ruiter P (2007) Spatial vegetation patterns and imminent desertification in Mediterranean arid ecosystems. Nature 449:213–217. https://doi.org/10.1038/nature06111
Lesschen J, Cammeraat L, Kooijman A, van Wesemael B (2008) Development of spatial heterogeneity in vegetation and soil properties after land abandonment in a semi-arid ecosystem. J Arid Environ 72:2082–2092. https://doi.org/10.1016/j.jaridenv.2008.06.006
Marasco A, Iuorio A, Carteni F, Bonanomi G, Tartakovsky DM, Mazzoleni S, Giannino F (2014) Vegetation pattern formation due to interactions between water availability and toxicity in plant-soil feedback. Bull Math Biol 76:2866–2883. https://doi.org/10.1007/s11538-014-0036-6
Meron E (2012) Pattern-formation approach to modelling spatially extended ecosystems. Ecol Model 234:70–82. https://doi.org/10.1016/j.ecolmodel.2011.05.035
Meron E (2018) From patterns to function in living systems: dryland ecosystems as a case study. Annu Rev Condens Matter Phys 9(79–103):033117–053959. https://doi.org/10.1146/annurevconmatphys-033117-053959
Miller P (2006) Applied asymptotic analysis. Graduate studies in mathematics. American Mathematical Society, New York. https://doi.org/10.1090/gsm/075
Murray J (1989) Mathematical biology. Springer, Berlin. https://doi.org/10.2307/2348289
Musgrave J, Lutscher F (2014a) Integrodifference equations in patchy landscapes I: dispersal kernels. J Math Biol 69:583–615. https://doi.org/10.1007/s00285-013-0714-2

Musgrave J, Lutscher F (2014b) Integrodifference equations in patchy landscapes II: population level consequences. J Math Biol 69:617–658. https://doi.org/10.1007/s00285-013-0715-1
Navarro T, Pascual V, Alados C, Cabezudo B (2009) Growth forms, dispersal strategies and taxonomic spectrum in a semi-arid shrubland in SE Spain. J Arid Environ 73:103–112. https://doi.org/10.1016/j.jaridenv.2008.09.009
Neubert M, Kot M, Lewis M (1995) Dispersal and pattern formation in a discrete-time predator–prey model. Theor Popul Biol 48:7–43. https://doi.org/10.1006/tpbi.1995.1020
Noy-Meir I (1973) Desert ecosystems: environment and producers. Annu Rev Ecol Syst 4:25–51. https://doi.org/10.1146/annurev.es.04.110173.000325
Parolin P (2006) Ombrohydrochory: rain-operated seed dispersal in plants with special regard to jet-action dispersal in Aizoaceae. Flora 201:511–518. https://doi.org/10.1016/j.flora.2005.11.003
Peel MC, Finlayson BL, McMahon TA (2007) Updated world map of the Köppen–Geiger climate classification. Hydrol Earth Syst Sci 11:1633–1644. https://doi.org/10.5194/hess-11-1633-2007
Powell JA, Zimmermann NE (2004) Multiscale analysis of active seed dispersal contributes to resolving Reid's Paradox. Ecology 85(490–506):0535. https://doi.org/10.1890/02-0535
Pueyo Y, Kéfi S, Alados CL, Rietkerk M (2008) Dispersal strategies and spatial organization of vegetation in arid ecosystems. Oikos 117:1522–1532. https://doi.org/10.1111/j.0030-1299.2008.16735.x
Pueyo Y, Kéfi S, Díaz-Sierra R, Alados C, Rietkerk M (2010) The role of reproductive plant traits and biotic interactions in the dynamics of semi-arid plant communities. Theor Popul Biol 78:289–297. https://doi.org/10.1016/j.tpb.2010.09.001
Rademacher JD, Sandstede B, Scheel A (2007) Computing absolute and essential spectra using continuation. Physica D 229:166–183. https://doi.org/10.1016/j.physd.2007.03.016
Rietkerk M, Ketner P, Burger J, Hoorens B, Olff H (2000) Multiscale soil and vegetation patchiness along a gradient of herbivore impact in a semi-arid grazing system in West Africa. Plant Ecol 148:207–224. https://doi.org/10.1023/A:1009828432690
Rietkerk M, Boerlijst MC, van Langevelde F, HilleRisLambers R, van de Koppel J, Kumar L, Prins HHT, de Roos AM (2002) Self-organization of vegetation in arid ecosystems. Am Nat 160:524–530. https://doi.org/10.1086/342078
Rietkerk M, Dekker SC, de Ruiter PC, van de Koppel J (2004) Self-organized patchiness and catastrophic shifts in ecosystems. Science 305:1926–1929. https://doi.org/10.1126/science.1101867
Rodriguez-Iturbe I, Porporato A, Ridolfi L, Isham V, Coxi DR (1999) Probabilistic modelling of water balance at a point: the role of climate, soil and vegetation. Proc R Soc Lond A 455:3789–3805. https://doi.org/10.1098/rspa.1999.0477
Rossi MJ, Ares JO (2017) Water fluxes between inter-patches and vegetated mounds in flat semiarid landscapes. J Hydrol 546:219–229. https://doi.org/10.1016/j.jhydrol.2017.01.016
Saco PM, Moreno M, Keesstra S, Baartman J, Yetemen O, Rodriguez JF (2018) Vegetation and soil degradation in drylands: non linear feedbacks and early warning signals. Curr Opin Environ Sci Health 5:67–72. https://doi.org/10.1016/j.coesh.2018.06.001
Salvucci GD (2001) Estimating the moisture dependence of root zone water loss using conditionally averaged precipitation. Water Resour Res 37:1357–1365. https://doi.org/10.1029/2000WR900336
Shabana HA, Navarro T, El-Keblawy A (2018) Dispersal traits in the hyper-arid hot desert of the United Arab Emirates. Plant Ecol Evol 151:194–208. https://doi.org/10.5091/plecevo.2018.1359
Sheffer E, Hardenberg J, Yizhaq H, Shachak M, Meron E, Blasius B (2013) Emerged or imposed: a theory on the role of physical templates and self-organisation for vegetation patchiness. Ecol Lett 16:127–139. https://doi.org/10.1111/ele.12027
Sherratt JA (2005) An analysis of vegetation stripe formation in semi-arid landscapes. J Math Biol 51:183–197. https://doi.org/10.1007/s00285-005-0319-5
Sherratt JA (2010) Pattern solutions of the Klausmeier model for banded vegetation in semi-arid environments I. Nonlinearity 23:2657–2675. https://doi.org/10.1088/0951-7715/23/10/016
Sherratt JA (2011) Pattern solutions of the Klausmeier model for banded vegetation in semi-arid environments II: patterns with the largest possible propagation speeds. Proc R Soc Lond A 467:3272–3294. https://doi.org/10.1098/rspa.2011.0194
Sherratt JA (2012) Numerical continuation methods for studying periodic travelling wave (wavetrain) solutions of partial differential equations. Appl Math Comput 218:4684–4694. https://doi.org/10.1016/j.amc.2011.11.005

Sherratt JA (2013a) Pattern solutions of the Klausmeier model for banded vegetation in semi-arid environments III: the transition between homoclinic solutions. Physica D 242:30–41. https://doi.org/10.1016/j.physd.2012.08.014
Sherratt JA (2013b) Pattern solutions of the Klausmeier model for banded vegetation in semiarid environments IV: slowly moving patterns and their stability. SIAM J Appl Math 73:330–350. https://doi.org/10.1137/120862648
Sherratt JA (2013c) Pattern solutions of the Klausmeier model for banded vegetation in semiarid environments V: the transition from patterns to desert. SIAM J Appl Math 73:1347–1367. https://doi.org/10.1137/120899510
Sherratt JA, Lord GJ (2007) Nonlinear dynamics and pattern bifurcations in a model for vegetation stripes in semi-arid environments. Theor Popul Biol 71:1–11. https://doi.org/10.1016/j.tpb.2006.07.009
Siero E (2018) Nonlocal grazing in patterned ecosystems. J Theor Biol 436:64–71. https://doi.org/10.1016/j.jtbi.2017.10.001
Siero E, Doelman A, Eppinga MB, Rademacher JDM, Rietkerk M, Siteur K (2015) Striped pattern selection by advective reaction-diffusion systems: resilience of banded vegetation on slopes. Chaos Interdiscip J Nonlinear Sci 25:036411. https://doi.org/10.1063/1.4914450
Siero E, Siteur K, Doelman A, van de Koppel J, Rietkerk M, Eppinga MB (2019) Grazing away the resilience of patterned ecosystems. Am Nat 193:472–480. https://doi.org/10.1086/701669
Siteur K, Siero E, Eppinga MB, Rademacher JD, Doelman A, Rietkerk M (2014a) Beyond Turing: the response of patterned ecosystems to environmental change. Ecol Complex 20:81–96. https://doi.org/10.1016/j.ecocom.2014.09.002
Siteur K, Eppinga MB, Karssenberg D, Baudena M, Bierkens MF, Rietkerk M (2014b) How will increases in rainfall intensity affect semiarid ecosystems? Water Resour Res 50:5980–6001. https://doi.org/10.1002/2013wr014955
Thompson SE, Harman CJ, Heine P, Katul GG (2010) Vegetation-infiltration relationships across climatic and soil type gradients. J Geophys Res Biogeosci 115:G02023. https://doi.org/10.1029/2009JG001134
Thompson S, Katul G, Konings A, Ridolfi L (2011) Unsteady overland flow on flat surfaces induced by spatial permeability contrasts. Adv Water Resour 34:1049–1058. https://doi.org/10.1016/j.advwatres.2011.05.012
United Nations Convention to Combat Desertification (2017) The global land outlook. Version first edition, Bonn, Germany
United Nations Food and Agriculture Organization (2005) Livestock sector briefs
Ursino N, Callegaro C (2016) Diversity without complementarity threatens vegetation patterns in arid lands. Ecohydrology 9:1187–1195. https://doi.org/10.1002/eco.1717
Ursino N, Contarini S (2006) Stability of banded vegetation patterns under seasonal rainfall and limited soil moisture storage capacity. Adv Water Resour 29:1556–1564. https://doi.org/10.1016/j.advwatres.2005.11.006
Valentin C, d'Herbès J, Poesen J (1999) Soil and water components of banded vegetation patterns. CATENA 37:1–24. https://doi.org/10.1016/S0341-8162(99)00053-3
van der Stelt S, Doelman A, Hek G, Rademacher JDM (2013) Rise and fall of periodic patterns for a generalized Klausmeier–Gray–Scott model. J Nonlinear Sci 23:39–95. https://doi.org/10.1007/s00332-012-9139-0
van Rheede van Oudtshoorn K, van Rooyen MW (2013) Dispersal biology of desert plants. Adaptations of desert organisms, Springer, Berlin
Wang W-J, Huai W-X, Thompson S, Katul GG (2015) Steady nonuniformshallowflow within emergent vegetation. Water Resour Res 51:10047–10064. https://doi.org/10.1002/2015wr017658
Wang X, Zhang G (2018) Vegetation pattern formation in seminal systems due to internal competition reaction between plants. J Theor Biol 458:10–14. https://doi.org/10.1016/j.jtbi.2018.08.043
Wang X, Zhang G (2019) The influence of infiltration feedback on the characteristic of banded vegetation pattern on hillsides of semiarid area. PLoS ONE 14:e0205715. https://doi.org/10.1371/journal.pone.0205715
Wang X, Lutscher F (2018) Turing patterns in a predator–prey model with seasonality. J Math Biol 78:711–737. https://doi.org/10.1007/s00285-018-1289-8
Zelnik YR, Kinast S, Yizhaq H, Bel G, Meron E (2013) Regime shifts in models of dryland vegetation. Philos Trans R Soc Lond Ser A 371:20120358. https://doi.org/10.1098/rsta.2012.0358
Zelnik YR, Gandhi P, Knobloch E, Meron E (2018) Implications of tristability in pattern-forming ecosystems. Chaos Interdiscip J Nonlinear Sci 28:033609. https://doi.org/10.1063/1.5018925

Affiliations

Lukas Eigentler[1,2,3] · Jonathan A. Sherratt[1]

✉ Lukas Eigentler
LEigentler001@dundee.ac.uk

Jonathan A. Sherratt
J.A.Sherratt@hw.ac.uk

1 Department of Mathematics, Maxwell Institute for Mathematical Sciences, Heriot Watt University, Edinburgh EH14 4AS, UK

2 Division of Molecular Microbiology, School of Life Sciences, University of Dundee, Dundee DD1 5EH, UK

3 Division of Mathematics, School of Science and Engineering, University of Dundee, Dundee DD1 4HN, UK